Journal of Rock Mechanics and Geotechnical Engineering 16 (2024) 1072–1084

Contents lists available at ScienceDirect

Journal of Rock Mechanics and Geotechnical Engineering

journal homepage: www.jrmge.cn

Full Length Article

Experimental investigation on the permeability of gap-graded soil due to horizontal suffusion considering boundary effect

Xuwei Wang [a,b], Yeshuang Xu [a,b,*]

[a] State Key Laboratory of Ocean Engineering, School of Naval Architecture, Ocean, and Civil Engineering, Shanghai Jiao Tong University, Shanghai, 200240, China
[b] Shanghai Key Laboratory for Digital Maintenance of Buildings and Infrastructure, Department of Civil Engineering, Shanghai Jiao Tong University, Shanghai, 200240, China

ARTICLE INFO

Article history:
Received 6 January 2023
Received in revised form
12 May 2023
Accepted 14 August 2023
Available online 22 November 2023

Keywords:
Suffusion
Permeability
Experimental investigation
Boundary effect
Horizontal seepage

ABSTRACT

The boundary condition is a crucial factor affecting the permeability variation due to suffusion. An experimental investigation on the permeability of gap-graded soil due to horizontal suffusion considering the boundary effect is conducted, where the hydraulic head difference (ΔH) varies, and the boundary includes non-loss and soil-loss conditions. Soil samples are filled into seven soil storerooms connected in turn. After evaluation, the variation in content of fine sand (ΔR_{f}) and the hydraulic conductivity of soils in each storeroom (C_i) are analyzed. In the non-loss test, the soil sample filling area is divided into runoff, transited, and accumulated areas according to the negative or positive ΔR_{f} values. ΔR_{f} increases from negative to positive along the seepage path, and C_i decreases from runoff area to transited area and then rebounds in accumulated area. In the soil-loss test, all soil sample filling areas belong to the runoff area, where the gentle-loss, strengthened-loss, and alleviated-loss parts are further divided. ΔR_{f} decreases from the gentle-loss part to the strengthened-loss part and then rebounds in the alleviated-loss part, and C_i increases and then decreases along the seepage path. The relationship between ΔR_{f} and C_i is different with the boundary condition. C_i exponentially decreases with ΔR_{f} in the non-loss test and increases with ΔR_{f} generally in the soil-loss test.

1. Introduction

Suffusion in soil induced by seepage flow is a typical internal erosion, meaning that movable fine particles selectively migrate through voids formed by coarse particles and the total volume of soil remains (Moffat and Fannin, 2006; Rochim et al., 2017). The suffusion process widely exists in hydraulic and geotechnical engineering (Dong et al., 2018; Yang et al., 2019a, 2019b; Fetrati and Pak, 2020; Wang et al., 2022), such as embankment dams, dikes, levees, foundation pits and tunnels (Foster et al., 2000; Xu et al., 2012, 2013; Wu et al., 2020b, c; Lyu et al., 2021, 2022). Suffusion is more likely to occur in gap-graded soil (Sibille et al., 2015; Yin et al., 2020; Yin and Wang, 2021), and the soil's permeability characteristics, such as particle redistribution, porosity, and hydraulic conductivity, vary during suffusion (Rochim et al., 2017; Li et al., 2023). These variations result in the degradation of the soil's mechanical properties, and specific disasters are likely to occur if the progressive degradation develops, such as collapsing dams, river banks, ground surfaces (Planes et al., 2016; Tan and Long, 2021; Wang and Xu, 2022), water inrush, and tunnel leakages (Wu et al., 2015, 2017; Tan and Lu, 2017; Ma et al., 2019).

Experimental investigations are convenient and practical to study the permeability variation of soil induced by different suffusion variables (Ke and Takahashi, 2014a, b; Cheng et al., 2017, 2018; Selvadurai and Głowacki, 2018; Benamar et al., 2019; Peng and Rice, 2020), such as the seepage direction (Hosn, 2017; Pachideh and Hosseini, 2018) and the boundary condition (Caldeira, 2019). Experiments based on vertical seepage have been conducted considerably (Chen et al., 2016; Liang et al., 2019; Luo et al., 2019), whereas horizontal seepage widely exists in hydraulic and geotechnical engineering, such as core-wall of embankment dams (Kim et al., 2022), bottom position below waterproof curtain (Xu et al., 2014, 2019; Wang et al., 2019; Wang and Xu, 2021; Zeng et al., 2021a, b, 2022) and middle positions of tunnels (Wu et al., 2020a). Compared to vertical suffusion, the soil's permeability

* Corresponding author. State Key Laboratory of Ocean Engineering, School of Naval Architecture, Ocean, and Civil Engineering, Shanghai Jiao Tong University, Shanghai, 200240, China.
E-mail address: xuyeshuang@sjtu.edu.cn (Y. Xu).
Peer review under responsibility of Institute of Rock and Soil Mechanics, Chinese Academy of Sciences.

https://doi.org/10.1016/j.jrmge.2023.08.017
1674-7755

changes easier under lower hydraulic gradients and distributes ununiformly after horizontal tests (Liang et al., 2020; Luo et al., 2020; Wang and Xu, 2023). Moreover, the eroded area develops gradually from the upper to the lower area, and the loss velocity of fine particles in the horizontal direction is slower than that in the vertical direction (Liang et al., 2022).

Furthermore, some studies proved the soil's ununiform permeability after suffusion under different boundary conditions (Ke and Takahashi, 2014a; Deng et al., 2020; Luo et al., 2020; Chen et al., 2021). These studies analyzed the permeability variation affected by a single boundary condition, including soil-loss (Sail et al., 2011; Zhong et al., 2018; Chen et al., 2021) or non-loss boundaries (Deng et al., 2020; Luo et al., 2020), respectively, where the soil-loss boundary means that fine particles can dislodge from the soil while the non-loss boundary limits the runoff of fine particles. Nevertheless, both boundaries can exist simultaneously during suffusion in practical engineering, such as embankment dams and tunnels (Pachideh and Hosseini, 2018; Yang et al., 2022). Some studies proposed that the variation in permeability characteristics of soil caused by suffusion under horizontal seepage at different boundary conditions should be studied further (Xiao and Shwiyhat, 2012; Pachideh and Hosseini, 2018).

This paper investigates the variation in soil permeability characteristics due to suffusion by conducting a horizontal seepage experiment considering different boundary conditions. First, the experimental apparatus and scheme are introduced. Then, the test results of the outflow rate, water level, and grading curve are illustrated. Next, the change rate of local fine particles and hydraulic conductivity are analyzed to investigate the permeability variations under different hydraulic head differences. Finally, the effect of the boundary condition on permeability variation is discussed.

2. Horizontal suffusion experiment

2.1. Experimental apparatus

Fig. 1 shows the sketch map and the picture of the experimental apparatus, which includes a water tank, a horizontal cylinder, water-level monitoring tubes, and a water-collect box with strainers. The water tank, with a length, width, and height of 300 mm, 300 mm, and 400 mm, respectively, provides constant hydraulic head difference (ΔH) during the experiment. A flexible pipe connects the water tank with a horizontal cylinder.

Table 1
The scheme of experiments.

ΔH (mm)	Non-loss test		Soil-loss test	
	Number	Outlet condition	Number	Outlet condition
300	U-1	Round plate with filter screen (d = 0.038 mm)	O-1	Round plate with horizontal seam (l = 1.3 mm)
450	U-2		O-2	
600	U-3		O-3	
750	U-4		O-4	
900	U-5		O-5	

The horizontal cylinder includes an inflow room, seven soil storerooms (labeled from S_1 to S_7 from upstream to downstream), and a round plate. The horizontal cylinder's diameter and total length are 80 mm and 960 mm, respectively. The inflow room and soil storerooms with a length of 120 mm each are connected in turn, and a round plate with a filter screen or horizontal seam is set at the tail of storeroom S_7 to simulate non-loss or soil-loss boundary conditions, respectively. This seam boundary is regarded as a kind of typical leakage type in geotechnical engineering, which can simulate the leakage condition of waterproof curtain in foundation pit engineering, the longitudinal joint of tunnel engineering, core-wall fissure of embankment dams, and so on.

Seven water-level monitoring tubes (labeled from h_1 to h_7) with a measuring range from 100 mm to 1000 mm are set at the middle point of corresponding soil storerooms (Fig. 1). The water-collection box with strainers is placed below the outlet of storeroom S_7, and strainers are set above the water-collect box to separate the dislodged particles and outflow water.

2.2. Experimental material and scheme

The experimental material includes coarse white sand and fine green sand. The grain size of coarse sand ranges from 1 mm to 5 mm, and that of fine sand ranges from 0.063 mm to 0.3 mm. Shire et al. (2014) proposed that internal erosion is more likely to occur in the soil with rate of fine particles less than 35%; thus, the mass percentage of fine sand (defined as R_f) is set as 15% in this experiment.

Table 1 tabulates the scheme of the suffusion experiment, including the non-loss and soil-loss tests. The ΔH value is the

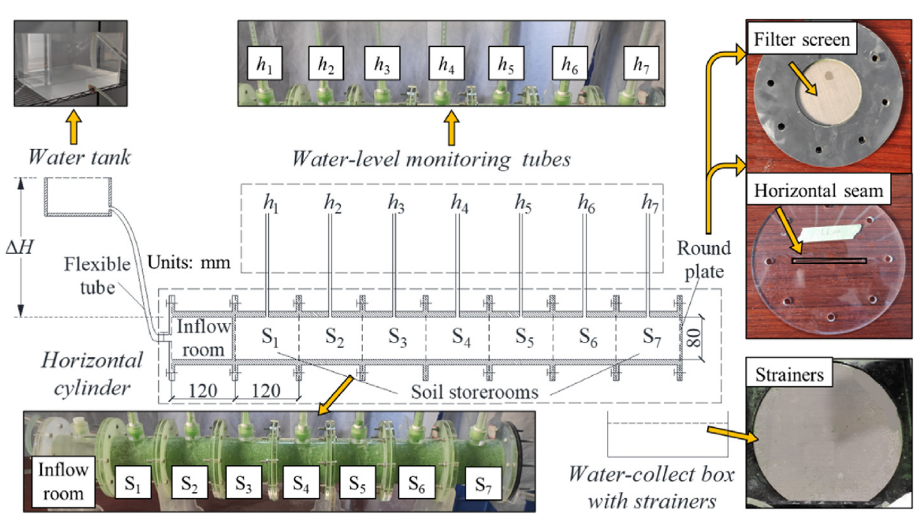

Fig. 1. Sketch map and pictures of the experimental apparatus.

experiment's variable, set as 300 mm, 450 mm, 600 mm, 750 mm, and 900 mm, respectively. The non-loss test includes five cases labeled from U-1 to U-5, and the round plate with a filter screen at the tail of storeroom S_7 controls the outlet condition, where the void diameter of the filter screen (d) is 0.038 mm to prevent soil loss. The soil-loss test includes five cases labeled from O-1 to O-5, and the round plate with a horizontal seam controls the outlet condition, where the seam width (l) is 1.3 mm, allowing fine sand to pass.

The weights of coarse and fine sands are the same in each case to ensure the consistency of mixed sand. The soil's physical properties include the dry density and specific gravity by measurement and the porosity by calculation. Three samples are taken in each case to measure the physical properties. The mixed sand is considered uniform when each sample's measuring error is smaller than 5%. Table 2 tabulates the parameters of the coarse, fine, and mixed soils, and Fig. 2 shows the grain size curves in each case. Based on the grading curves, the mixed sample accords with the gap-graded soil according to the division in ASTM D2487 (2011).

Table 3 illustrates the soil mass in each storeroom before test under non-loss or soil-loss boundary. The standard soil mass in each storeroom is approximately 1.1 kg under same operation procedure, in which the maximum error in storerooms is 0.017 kg, 0.022 kg, 0.021 kg, 0.017 kg, and 0.016 kg in the non-loss test, and the corresponding error is 0.018 kg, 0.023 kg, 0.018 kg, 0.017 kg and 0.015 kg in the soil-loss test. Because the mass of coarse and fine sand, the stirring, filling and saturating procedure is tried to keep consistent, the porosity of sample in each storeroom is considered the same.

2.3. Experimental procedure

The experimental procedure is introduced as follows:

(1) Filling and saturating soil: after smearing vaseline on the inner face of apparatus to avoid contact erosion, the mixed soil is filled in a storeroom layer by layer with a thickness of 20 mm, and then the soil is saturated. Next, the storeroom filled with soil is connected to another storeroom. Soil filling, saturation, and storeroom connection are operated repeatedly until the soils in the seven storerooms are filled and saturated.

(2) Assembling the apparatus: a horizontal cylinder is formed by connecting the inflow room and soil storerooms, and the inflow room filled with water is connected to the water-supply system. Seven monitoring tubes are assembled at the middle point of each soil storeroom. An additional round plate is set at the tail of horizontal cylinder preventing runoff of water before test. The water tank is lifted to a specific height to provide a constant ΔH value. Test cases begin only when the water level of seven monitoring tubes (from h_1 to h_7) equals the water tank's height.

(3) Experimental process: each case in Table 1 is conducted three times to reduce test errors, and each test case lasts 3 h. During the experimental process, the water-level data of seven monitoring tubes (from h_1 to h_7) are recorded every 15 min, and the outflow rate in 1 min (Q) is measured by measuring the cylinder simultaneously. Strainers above the water-collection box collect the dislodged particles in the soil-loss test. Soil samples in each storeroom are collected separately after each test case to obtain the grain size curves.

Table 2
Parameters of sandy soil.

Parameter	Value		
	Coarse sand	Fine sand	Mixed sand
Mass, m (kg)	6.8	1.2	8
Dry density, ρ_d (g/cm^3)	1.48	1.84	1.81
Porosity, n	0.45	0.31	0.32
Specific gravity, G_s	2.65	2.66	2.65
Effective grain size, d_{10} (mm)	1.394	0.055	0.158
Continuous grain size, d_{30} (mm)	2.016	0.069	2.014
Constrained grain size, d_{60} (mm)	2.232	0.111	2.971
Coefficient of uniformity, C_u	1.6	2.03	18.9
Coefficient of curvature, C_c	1.31	0.78	8.67

3. Experiment results

3.1. Suffusion phenomena at the outlet

Fig. 3 shows a picture of suffusion phenomena at storeroom S_7 in cases U-5 and O-5. Coarse white and fine green sands are uniformly distributed before the test (Fig. 3a). After the non-loss test, the green sand area increases noticeably due to the limitation of a filter screen at the tail, where the fine sands accumulate (Fig. 3b). However, after the soil-loss test, the proportion of coarse white sand increases (Fig. 3c) because the fine sands dislodge (Fig. 3d). Since the width of horizontal seam is 1.3 mm, smaller than d_{10} of coarse sand, it is reasonable to consider there is no loss of coarse sand, and only fine green sand can dislodge.

The soil mass in each soil storeroom after the test is tabulated in Table 4. The total mass difference of the soil in all soil storerooms before and after the test (W_t) is smaller than 0.005 kg in non-loss test and that is 0.099 kg, 0.166 kg, 0.190 kg, 0.224 kg and 0.256 kg in soil-loss test. W_t in soil-loss test is closed to the weight of the soil collected by the strainer shown in Fig. 3d, which are 0.097 kg, 0.163 kg, 0.189 kg, 0.221 kg and 0.255 kg, respectively. Fig. 4 shows the grading curves of dislodged particles. The curves shift down with the increasing ΔH and the increasing proportion of particles with large diameters. Besides, the percentage of dislodged particles (P_d), defined as the weight ratio of dislodged particles and original fine sand, is obtained as shown in Fig. 5. The value of P_d increases from 1.29% to 3.31% when ΔH increases from 300 mm to 900 mm. That is to say, with the increasing ΔH, P_d increases due to increasing water pressure.

3.2. Outflow rate

Fig. 5 shows the change in Q with time (T), in which the variation tendency of Q differs with boundaries. In the non-loss test, the value of Q varies from 15.2 mL/min to 12.4 mL/min and from 47 mL/min to 44.3 mL/min when ΔH is 300 mm or 450 mm, respectively, and the corresponding difference is only 2.8 mL/min and 2.7 mL/min. This phenomenon indicates the suffusion process is relatively gentle under the comprehensive effect of low ΔH and non-loss boundary generally. When ΔH is 600 mm, Q increases from 102.7 mL/min to 114.6 mL/min with little fluctuation, reflecting the suffusion process enhances with increasing ΔH. When ΔH is 750 mm or 900 mm, Q increases over time obviously first and then remains stable, and the corresponding increment is 73.1 mL/min and 57.8 mL/min, respectively, indicating that the suffusion process results in obvious variation in permeability of soils.

In the soil-loss test, all the values of Q are also larger than that in corresponding cases of non-loss test, indicating that the suffusion process is easier to develop under the soil-loss boundary compared with the non-loss boundary. When ΔH is 300 mm or 450 mm, the value and change in Q are also small and the suffusion process is also relatively gentle. When ΔH is larger than 450 mm, Q decreases near-linearly with the increasing ΔH. The value of Q is 154 mL/min,

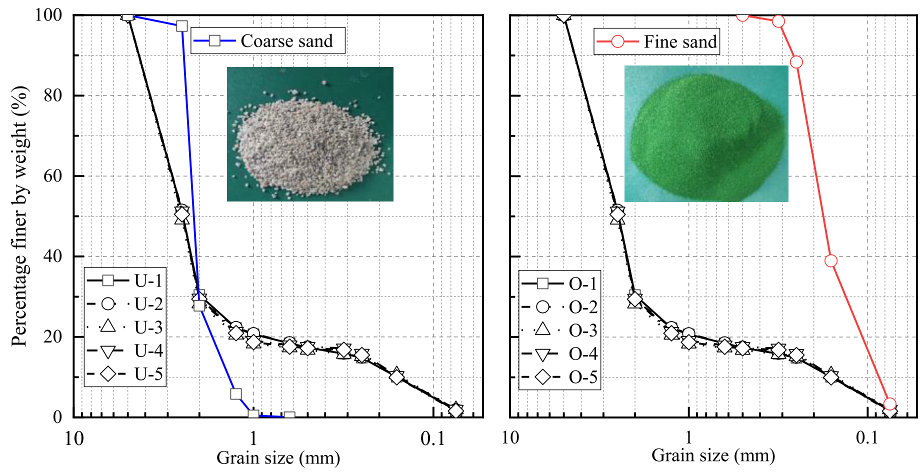

Fig. 2. Grain size curves of soil sample.

Table 3
Soil mass in each storeroom before the test.

Soil storeroom	Soil mass in non-loss test (kg)					Soil mass in soil-loss test (kg)				
	U-1	U-2	U-3	U-4	U-5	O-1	O-2	O-3	O-4	O-5
S_1	1.108	1.109	1.114	1.097	1.102	1.098	1.115	1.088	1.108	1.095
S_2	1.092	1.09	1.105	1.104	1.089	1.092	1.101	1.103	1.104	1.11
S_3	1.115	1.112	1.093	1.108	1.105	1.1	1.092	1.096	1.098	1.096
S_4	1.103	1.101	1.106	1.096	1.097	1.092	1.1	1.097	1.091	1.096
S_5	1.098	1.1	1.103	1.095	1.103	1.104	1.107	1.101	1.1	1.109
S_6	1.1	1.096	1.098	1.1	1.101	1.11	1.093	1.106	1.096	1.1
S_7	1.099	1.096	1.098	1.112	1.102	1.102	1.096	1.104	1.097	1.102
Total	7.715	7.704	7.717	7.712	7.699	7.698	7.704	7.695	7.694	7.708

179.6 mL/min, and 292 mL/min at 5 min and decreases to 122.5 mL/min, 146.4 mL/min, and 254.3 mL/min at 180 min when ΔH is 600 mm, 750 mm, and 900 mm, respectively.

3.3. Water level

Fig. 6 shows the observed water-level variations of the monitoring tubes (h) with T and L in Case U-5, where L is defined as the distance away from the left side of storeroom S_1. An additional round plate is set at the tail of horizontal cylinder preventing runoff of water before experiment. The water tank is slowly lifted to 900 mm before moving away the additional round plate, hence all the values of h in the monitoring tubes are 900 mm at start time.

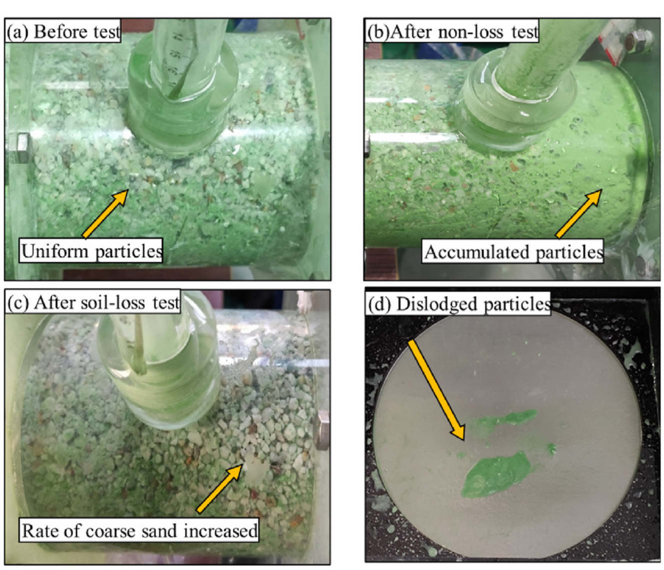

Fig. 3. Picture of suffusion phenomena at storeroom S_7 in cases U-5 and O-5.

Fig. 6a shows that h decreases first because the original voids may be occupied and even blocked by migrated fine sands, then h recovers because the blocked voids may open with the continuous scouring effect, and h increases slowly indicating that the suffusion process tends to be steady. This phenomenon is also proved by some researches (Ke and Takahashi, 2014a; Sibille et al., 2015; Rochim et al., 2017; Deng et al., 2020). The increasing velocity of h slows after 105 min, indicating a steady suffusion process. For example, h_7 decreases from 605 mm at 5 min to 513 mm at 30 min, recovers to 593 mm at 105 min and then increases to 623 mm at 180 min.

Fig. 6b shows that the relationship between h and L at 5 min and 45 min can be fitted linearly, indicating the permeability uniformly distributes. The variation rate of h with L increases from 37.8% at 5 min to 48.9% at 45 min. With continuous suffusion, the linear correlation of h and L weakens, and the distribution of h after 105 min can be divided into three parts. The slope of h from storerooms S_1 to S_3 is larger than the slope from storerooms S_3 to S_6, and the slope from storerooms S_6 to S_7 recovers. This phenomenon presents at 180 min, indicating the permeability is not uniformly distributed along the seepage path after suffusion.

Fig. 7 shows the variation in h with T and L in case O-5. All h decreases quickly in first 5 min because the soil-loss boundary allows both soil and water pass, then h increases gently with the increasing T after 5 min (Fig. 7a) since the continuous scouring effect. Due to the limitation of the monitoring tubes' measuring

Table 4
Soil mass in each storeroom after the test.

Soil storeroom	Soil mass in non-loss test (kg)					Soil mass in soil-loss test (kg)				
	U-1	U-2	U-3	U-4	U-5	O-1	O-2	O-3	O-4	O-5
S_1	1.105	1.106	1.103	1.077	1.081	1.093	1.102	1.076	1.095	1.077
S_2	1.09	1.089	1.094	1.088	1.068	1.083	1.085	1.088	1.086	1.09
S_3	1.114	1.111	1.083	1.094	1.087	1.091	1.075	1.08	1.074	1.071
S_4	1.102	1.1	1.101	1.087	1.082	1.077	1.081	1.076	1.063	1.064
S_5	1.097	1.098	1.101	1.089	1.093	1.083	1.072	1.058	1.053	1.054
S_6	1.102	1.099	1.112	1.122	1.133	1.087	1.056	1.061	1.047	1.045
S_7	1.1	1.1	1.116	1.153	1.152	1.086	1.067	1.065	1.053	1.052
Total	7.709	7.703	7.712	7.71	7.697	7.599	7.538	7.505	7.47	7.452
W_t	0.006	0.001	0.005	0.002	0.002	0.099	0.166	0.19	0.224	0.256

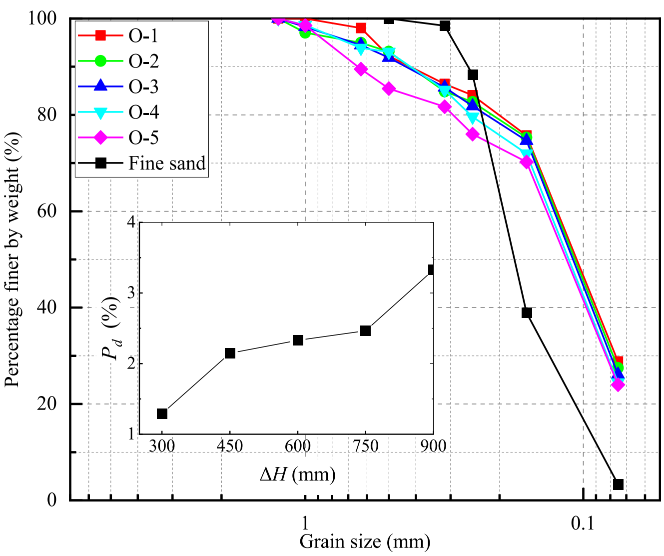

Fig. 4. Grading curves and loss rate of dislodged particles after the soil-loss test.

range where only value of h over 100 mm can be measured, the value of h_7 for the first 90 min which under 100 mm is not shown in Fig. 7a.

Fig. 7b shows the relationship between h and L in case O-5. The relationship between h and L at 5 min can be fitted linearly with a slope of −1.066, indicating that the drawdown of h is approximately 106.6 mm with each increase in L in 100 mm. This phenomenon indicates that although the local permeability of soil varies in the suffusion process, the general permeability of soil is also in accordance with the Darcy' law. With continuous suffusion, the variation rate of h along L decreases with T, i.e. the permeability enhances gradually at the soil-loss boundary because the loss of h in unit L decreases. Furthermore, the local permeability of soil presents obvious difference after suffusion experiment. For example, the distribution of h at 180 min can be divided into two parts. The fitting line slope from storerooms S_1 to S_4 is −0.907, while that from storerooms S_5 to S_7 is −1.092, indicating that the permeability of soil in storerooms S_5 to S_7 is larger than that in storerooms S_1 to S_4 after the soil-loss test. However, the phenomenon of local variation in permeability of soil under soil-loss boundary is not obvious compared with that under the non-loss boundary, which may be attributed to the accumulation degree of fine sand that is not strong.

3.4. Grading curve

The bolts connected two adjacent soil-storage chambers are released after the tests, and a very thin sheet iron is penetrated into the small gap formed by release to separate soil samples in each storeroom, then the grain size curves of the soil in each storeroom after the test is obtained. Fig. 8 shows the grain size curves after the test in cases U-5 and O-5, where all grain size curves vary from the original curve (labeled S_{og}), and the value of fine sand of each curve are listed to present the change in content of fine sand. Since each soil storeroom's original curves before the test are very close, the curve S_{og} is taken by the mixed sand before the corresponding test (Fig. 2). The coarse particles are considered static, and the fine sand

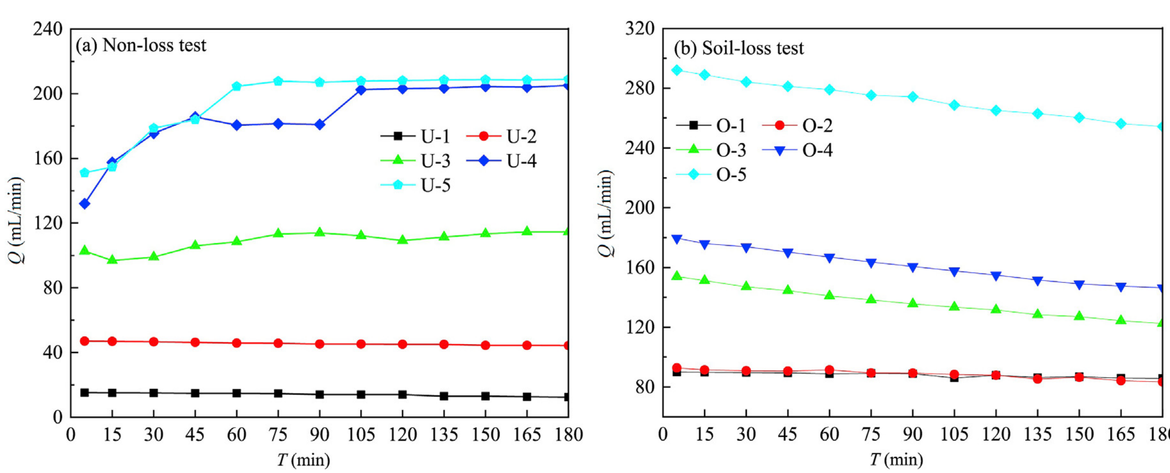

Fig. 5. Variation in Q with T: (a) Non-loss test, and (b) Soil-loss test.

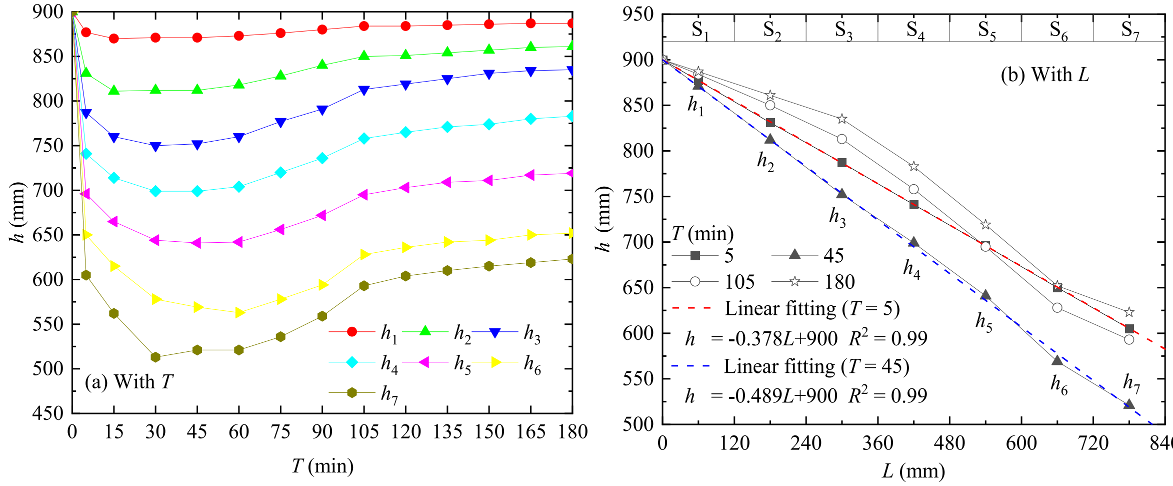

Fig. 6. Variation in h in case U-5: (a) With T, and (b) With L.

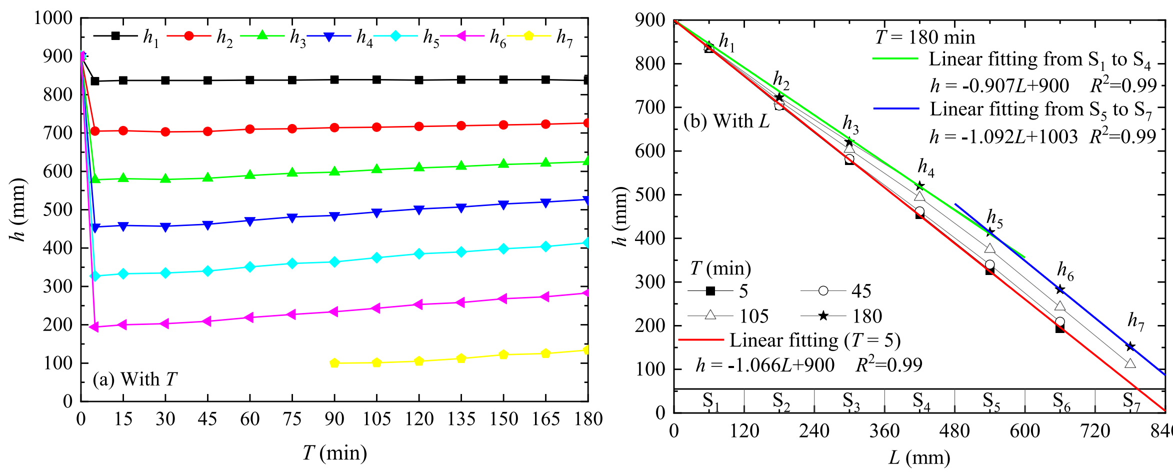

Fig. 7. Variation in h in case O-5: (a) With T, and (b) With L.

are considered movable. Hence, the migration and loss of fine sand cause different curves at different positions. Fig. 8a shows that the curves of storerooms S_6 and S_7 shift up, reflecting the accumulation of fine sand after the non-loss test. The curves from storerooms S_1 and S_5 shift down, reflecting the dislodgement of fine sand, and the dislodged degree decreases along the seepage path before storeroom S_5.

Fig. 8b shows that all curves shift down compared with the S_{og}, indicating the dislodgment of fine sand after the soil-loss test. The dislodged degree of fine sand decreases slightly along the seepage path from storerooms S_1 to S_6. It is worth mentioning that because the horizontal seam is at the middle height of the round section in storeroom S_7, the fine sand at the lower semicircle cannot run off, and the dislodged degree of fine sand is smaller than that in storerooms S_5 and S_6. Therefore, the dislodged boundary's shape influences the dislodged degree of particles significantly, and this conclusion correlates with the research by Zhang et al. (2019).

4. Investigation on the permeability variation due to suffusion

Under different values of ΔH, the migration of fine sand results in nonuniform distribution inside the soil along the seepage path, influencing the permeability of sandy soil. The indices related to soil permeability, including the variation content of fine sand (labeled ΔR_f) and change rate of hydraulic conductivity (labeled C_i), will be analyzed below. The ΔR_f at a specific position is defined as

$$\Delta R_f = R_f' - R_f \tag{1}$$

where R_f' is the content of fine sand after the non-loss or soil-loss tests at a specific position. These two parameters are obtained from the corresponding grading curve. The hydraulic conductivity of soils in each storeroom (labeled k_i) can be calculated using Darcy's law, and the change rate of k_i (labeled C_i) is defined as

$$\left.\begin{aligned} \Delta h_i &= \frac{h_{i-1}+h_i}{2} - \frac{h_i+h_{i+1}}{2} \\ k_i &= \frac{Q\Delta L_i}{A\Delta h_i} \\ C_i &= \frac{k_i'-k_i}{k_i} \end{aligned}\right\} \tag{2}$$

where Δh_i is the difference in water levels in storeroom S_i, and the water levels at both ends are calculated using linear interpolation of the observed data; A is the seepage section area; ΔL_i is each

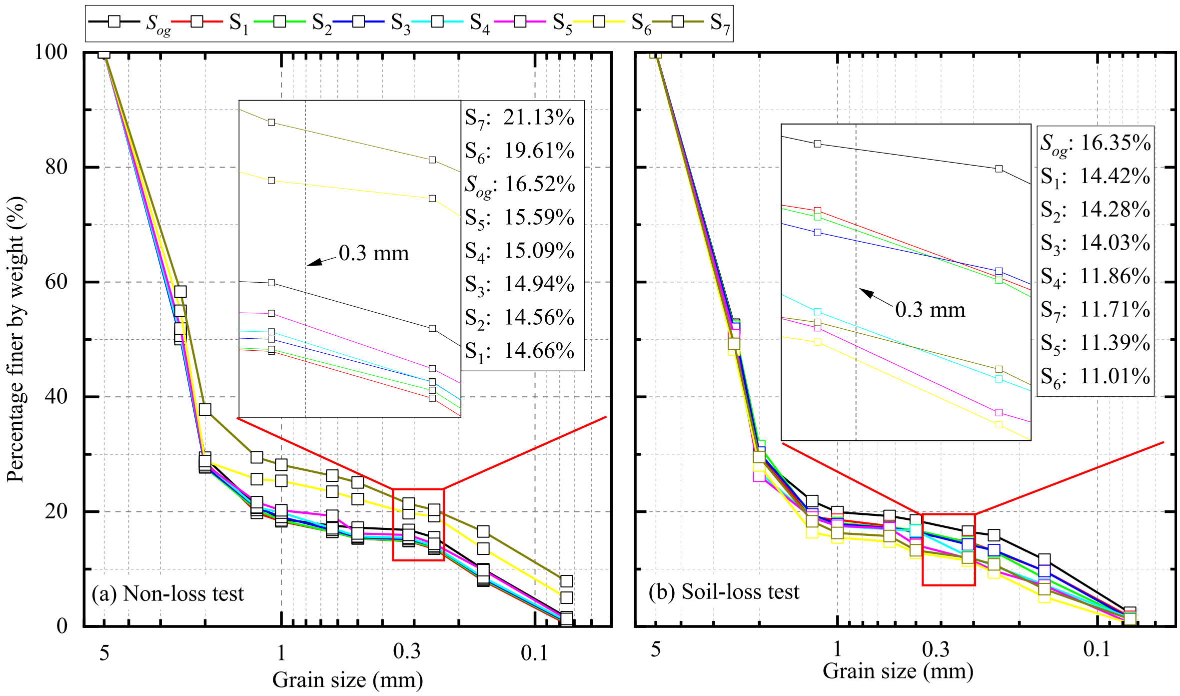

Fig. 8. Grain composition after the test: (a) Case U-5, and (b) Case O-5.

storeroom's seepage length; and k_i' is the hydraulic conductivity after the test. Since the hydraulic head at the inlet position of storeroom S_1 can be seen as a constant value, k_1 is calculated by the difference between the hydraulic head at the inlet and the average values of h_1 and h_2.

4.1. Non-loss boundary test

4.1.1. Investigation on ΔR_f

Fig. 9 shows the variation in ΔR_f with L after the non-loss test and all ΔR_f increase from negative to positive. According to the positive and negative values of ΔR_f, three areas can be divided along the seepage path: runoff, transited, and accumulated. The runoff area with negative values of ΔR_f ranges from storerooms S_1 to S_4, and the accumulated area with positive values of ΔR_f includes storerooms S_6 and S_7. There should exist a value where ΔR_f transfers from negative to positive value, and this point varies with different values of ΔH. By linear connection, all the X-coordinates of the point where ΔR_f equals zero all locate in storeroom S_5, and the values are 593.6 mm, 588.6 mm, 552.9 mm, 566.6 mm and 567.7 mm when ΔH increases from 300 mm to 900 mm. Storeroom S_5 is the transited area because the state of fine sand changes from the runoff condition to the accumulated condition in the non-loss test case.

When ΔH is low (300 mm or 450 mm), all ΔR_f values are smaller than 0.5%, indicating a slight migration degree of fine sand. Then, the distribution of ΔR_f in the runoff area shifts down with the

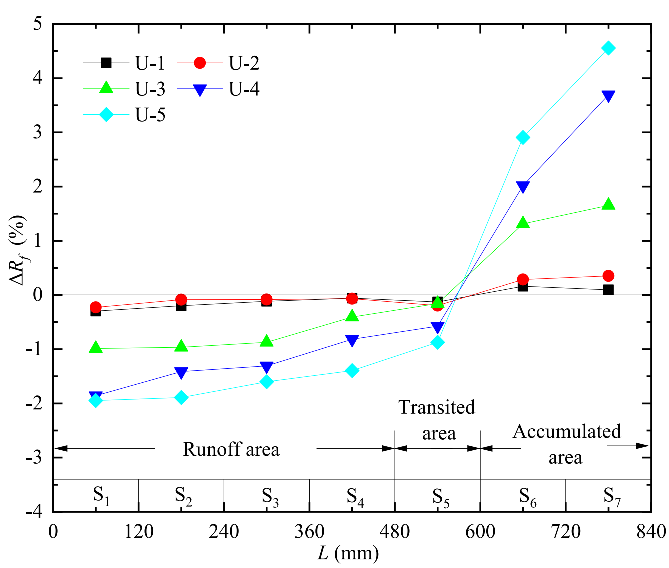

Fig. 9. Variation in ΔR_f with L after non-loss test.

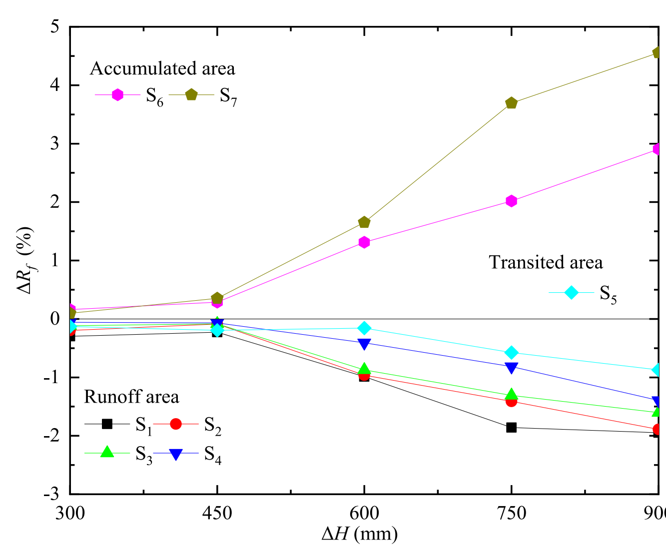

Fig. 10. Variation in ΔR_f with ΔH after non-loss test.

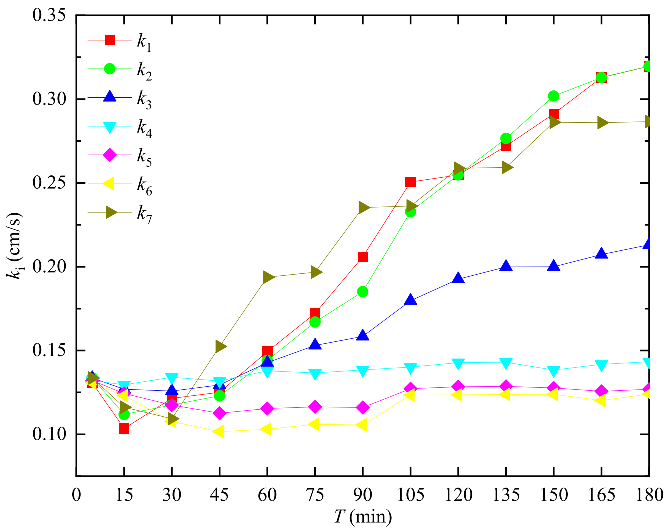

Fig. 11. Variation in k_i with T in case U-5.

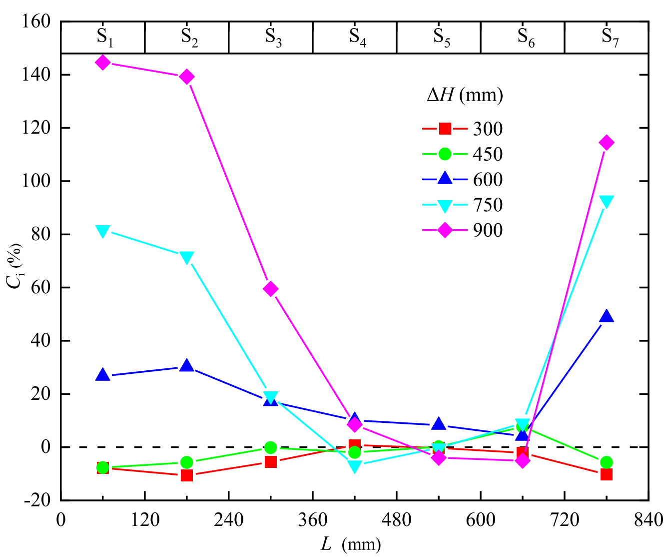

Fig. 12. Distribution of C_i with L after non-loss test.

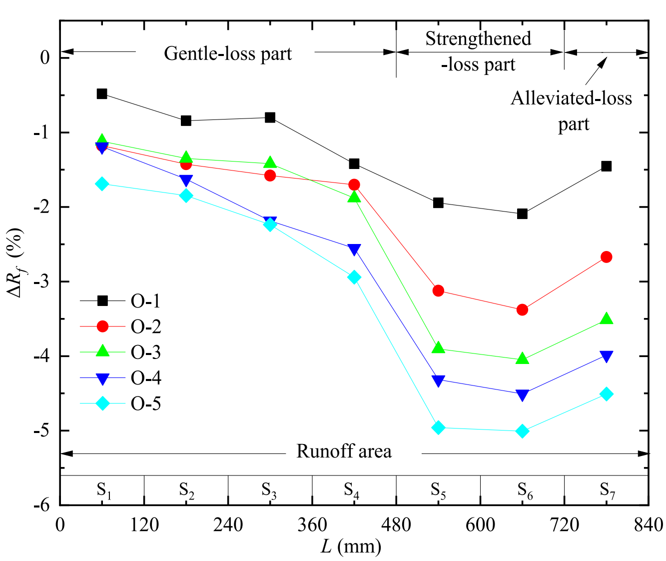

Fig. 13. Variation in ΔR_f with L after soil-loss test.

increasing ΔH, whereas the distribution of ΔR_f in the accumulated area shifts up with the increasing ΔH. The minimal and maximal values of ΔR_f occur at storerooms S_1 and S_7, where the loss and accumulated degree of particles are the most severe. The difference value of ΔR_f between storerooms S_1 and S_7 increases from 0.39% to 6.5% when ΔH increases from 300 mm to 900 mm, indicating that the migration degree of fine sand enhances with increasing ΔH.

Fig. 10 shows the variation in ΔR_f with ΔH. The variation tendency of ΔR_f in different areas significantly differ. When ΔH is low (300 mm or 450 mm), the ΔR_f values in all storerooms are small, indicating that the movement of fine sand slightly influences the ΔR_f. When ΔH is larger than 450 mm, ΔR_f in the runoff and transited areas decreases, whereas that in the accumulated area increases with the increasing ΔH, and the variation of ΔR_f in the transited area is smaller than that in the runoff area. For example, when ΔH increases from 450 mm to 900 mm, ΔR_f in storeroom S_4 of the runoff area approximately linearly decreased from -0.07% to -1.39%, ΔR_f in storeroom S_5 of the transited area only decreased from -0.20% to -0.87%, and ΔR_f in storeroom S_6 of the accumulated area increased from 0.29% to 2.91%. The corresponding variation rates of ΔR_f in storerooms S_4, S_5 and S_6 are -0.29%, -0.15% and 0.58%, respectively, with each increase in ΔH equal to 100 mm.

4.1.2. Investigation on C_i

Fig. 11 shows the variation in k_i with T in case U-5. In the runoff area from storerooms S_1 to S_4, k_i decreases and then increases obviously with time, which can be caused by the rearrangement of fine sand first and the migration of fine sand next. The increasing degree of k_i at 180 min along the seepage path decreases, correlating with the values of ΔR_f from storerooms S_1 to S_4. In the transited area, due to the accumulated particles from storeroom S_1 to S_4, and the fine sand here could migrate to storerooms S_6 and S_7, the variation in k_5 is small. Moreover, since the calculation process from k_4 to k_6 involves the water-level value in the transited area S_5, the variation also fluctuates little, and the variation degree is small. In the accumulated area of storeroom S_7, k_7 increases due to the rebound of h_7 values because of the boundary effect at the tail of storeroom S_7.

Fig. 12 shows the distribution of C_i with L after non-loss test. When ΔH is low (300 mm or 450 mm), C_i fluctuates with L because the suffusion degree is relatively small, and all the absolute values of C_i are smaller than 10%. In other tests with high ΔH values (from 600 mm to 900 mm), the variation in C_i along the seepage path differs, decreasing from the runoff area to the transited area and rebounding in the accumulated area. From storerooms S_1 to S_3, the values of C_i are large because of the loss of fine sand. The calculation process of the values from C_4 to C_6 involves the data in the transited area S_5; hence, all the values from C_4 to C_6 are smaller than 10%. The rebound of water level h_7 causes the C_7 rebound value in the accumulated area. For example, when ΔH is 900 mm, fine sand from storerooms S_1 to S_4 migrate to storerooms after, and C_i decreases from 144.6% to 59.52%. From storerooms S_4 to S_6, trough occurs as the values from C_4 to C_6 are 8.46%, -3.96% and -5.08%, respectively. Due to the influence of the boundary effect mentioned above, C_7 is large, with a value of 114.53%.

4.2. Soil-loss boundary test

4.2.1. Investigation on ΔR_f

Fig. 13 shows the variation in ΔR_f with L after the soil-loss test, decreasing with the increasing L from storerooms S_1 to S_6 and recovering at storeroom S_7. Since the soil-loss boundary allows fine sand to pass, all ΔR_f values are negative, indicating that all the storerooms belong to the runoff area. According to the suffusion degree, three parts can be divided: the gentle-loss part from

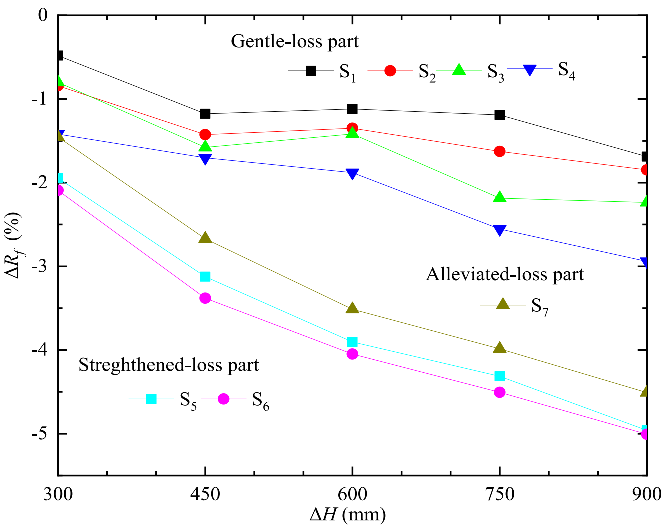

Fig. 14. Variation in ΔR_f with ΔH after soil-loss test.

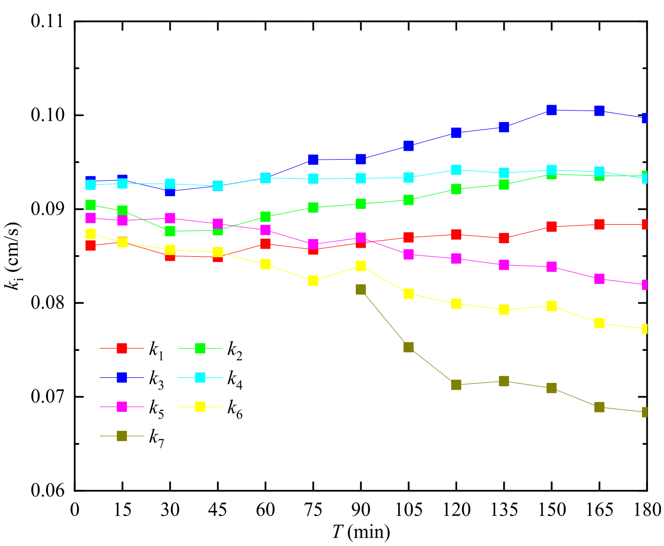

Fig. 15. Variation in k_i with T in case O-5.

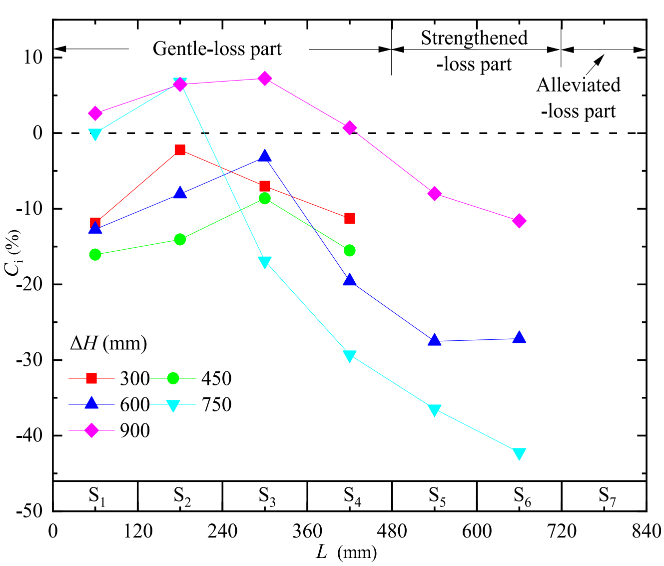

Fig. 16. Distribution of C_i with L after soil-loss test.

storerooms S_1 to S_4, the strengthened-loss part from storerooms S_5 to S_6, and the alleviated-loss part in storeroom S_7. The gentle-loss part is far from the soil-loss boundary, and ΔR_f decreases slightly with L. The decrease in ΔR_f in the strengthened-loss part is noticeable compared to that in the gentle-loss part. Since the horizontal seam is in the middle height of the round section and the fine sand at the lower semicircle in storeroom S_7 cannot run off, the value of ΔR_f rebounds in the alleviated-loss part.

Fig. 14 shows the variation in ΔR_f with ΔH after the soil-loss test. In the gentle-loss part, ΔR_f decreases with the increasing ΔH, and all the absolute values are smaller than 3%, indicating that the dislodged degree and the influence of the soil-loss boundary are small. In the strengthened-loss part, ΔR_f decreases with the increasing ΔH, and the values are much smaller than in the gentle-loss part. All the minimal values of ΔR_f occur in storeroom S_6, decreasing from −2.09% to −5.01% as ΔH increases from 300 mm to 900 mm. In the alleviated-loss part, the fine sand at the lower semicircle cannot run off due to the horizontal seam's limitation. Although ΔR_f decreases with the increasing ΔH, the values of ΔR_f in storeroom S_7 decrease from −1.45% to −4.51% as ΔH increases from 300 mm to 900 mm, of which the change value of ΔR_f is the largest in all the storerooms.

4.2.2. Investigation on C_i

Fig. 15 shows the variations in k_i with T in case O-5. In the gentle-loss part, k_i fluctuates with T, and the value at 180 min increases because of the dislodged particles. Tang et al. (2023) proposed that a dense filtering area could occur around the leakage boundary because of the local clogging phenomenon; hence, the soil permeability around the soil-loss boundary might decrease. The variation in k_i in the strengthened-loss part decreases with T. Although the observed data in storeroom S_7 only started from 90 min because of the monitoring range limitation, the decreasing degree of k_7 in the alleviated-loss part is more noticeable than that in the strengthened-loss part.

Fig. 16 shows the distribution of C_i with L after the soil-loss test, and there is a lack of observed data in storeroom S_7. All values of C_i increase and then decrease along the seepage path. In the gentle-loss part, the maximal value occurs at C_2 or C_3, and values at C_1 or C_4 are small. In the strengthened-loss part, C_i decreases with the increasing L, indicating that the soil-loss boundary's influence increases closer to the boundary.

5. Discussion on the effect of the boundary condition

5.1. Comparison of ΔR_f

Fig. 17 compares the ΔR_f between the non-loss and soil-loss boundaries. The tendency of ΔR_f can be classified into two types according to the variation tendency of ΔR_f: the similar-effect area from storerooms S_1 to S_5 and the reverse-effect area from storerooms S_6 to S_7. The variation tendency of ΔR_f in the similar-effect area both decreases with the increasing ΔH under the non-loss and soil-loss boundaries. Moreover, the differences in ΔR_f in the same storeroom under the non-loss and soil-loss boundaries (labeled R_{ns}) increase with L. For example, the value of R_{ns} is −0.26%, −0.04%, 0.63%, 1.55% and 4.19%, respectively, from storerooms S_1 to S_5 when ΔH is 900 mm, indicating that the boundary's influence enhances gradually.

In the reverse-effect area, the variation tendency of ΔR_f owns opposite variations, where ΔR_f increases with ΔH under the non-loss boundary and decreases with ΔH under the soil-loss boundary. This phenomenon means that the boundary condition changes the suffusion mode of fine sand inside coarse matrix particles in storerooms S_6 and S_7. For example, R_{ns} increases from 1.55% to

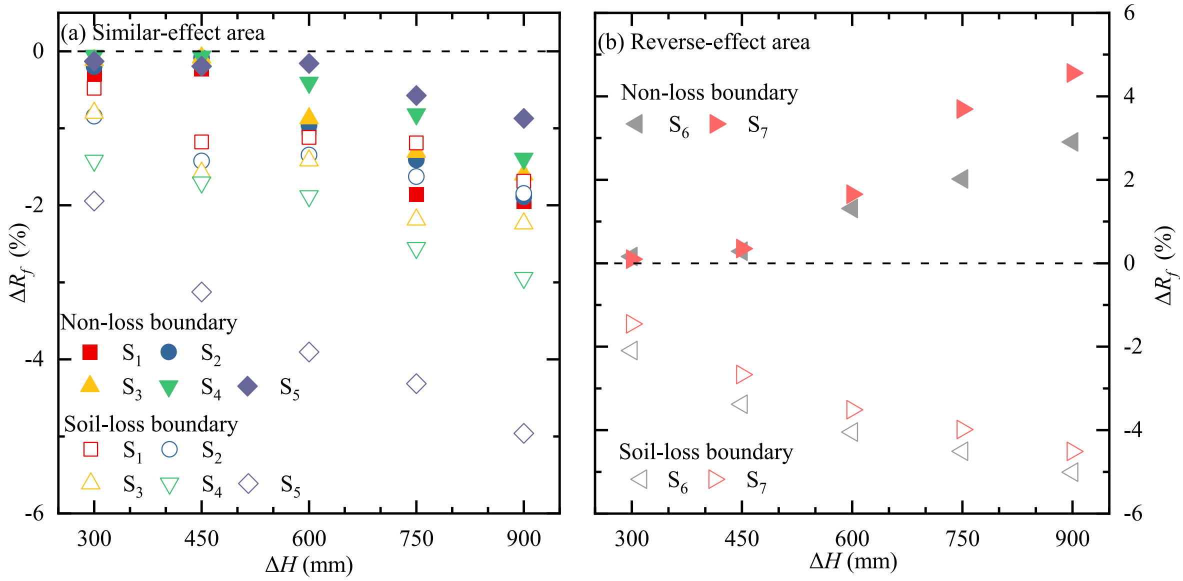

Fig. 17. Comparison of ΔR_f between non-loss and soil-loss tests.

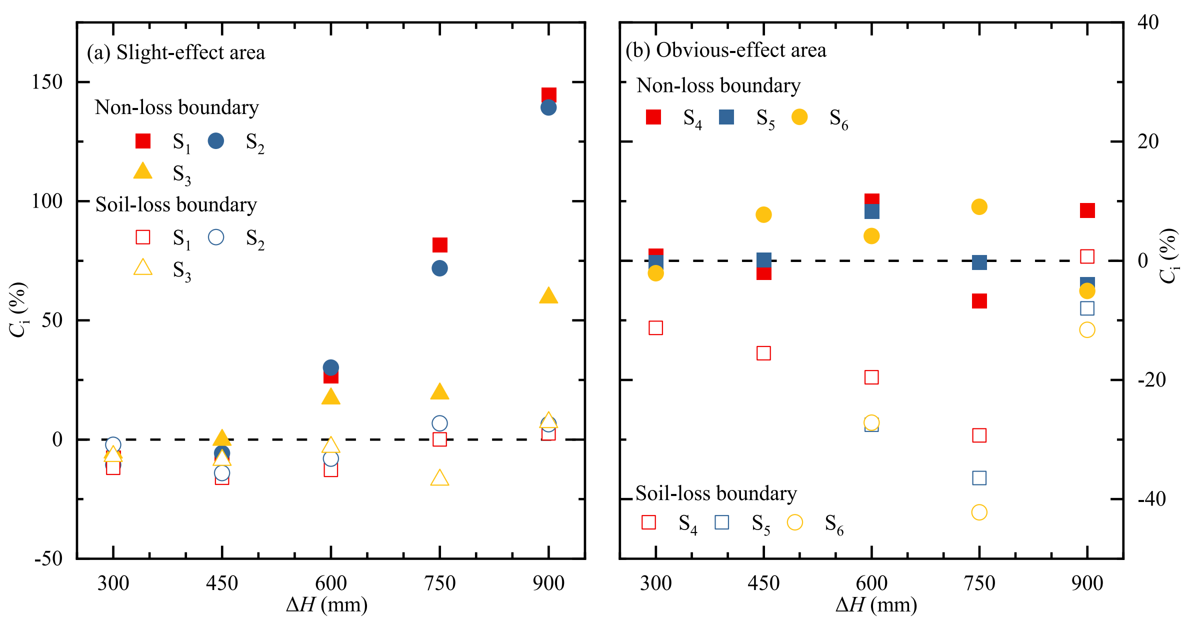

Fig. 18. Comparison of C_i between non-loss and soil-loss tests.

9.07% in storerooms S_7 when ΔH increases from 300 to 900 mm, much larger than R_{ns} in other storerooms. Liang et al. (2022) found out about 4.55% of fine sand dislodged in horizontal seepage test under soil-loss boundary, where the boundary is holes with a diameter of 0.075 mm distributed uniformly in cross-section. There is a slight difference between the values with 3.31% in the case O-5 because of the different soil-loss boundary.

5.2. Comparison of C_i

Fig. 18 compares the C_i between the non-loss and soil-loss tests. Unlike the influence of the boundary condition on ΔR_f, the similar-effect area from storerooms S_1 to S_3 and the reverse-effect area from storerooms S_4 to S_7 are divided. In the similar-effect area, the variation tendency of C_i increases with the increasing ΔH, where the increase under the non-loss test is noticeable, whereas the increase under the soil-loss test fluctuates. The value of C_i in the non-loss test varies from −10.65% to 144.6%, whereas C_i varies from −16.07% to 7.23% in the soil-loss test. This phenomenon means that the suffusion process primarily enhances the local seepage ability of soil from storerooms S_1 to S_3 in the non-loss test, whereas the local seepage ability in the soil-loss test is mostly weakened.

In the reverse-effect area, the variation tendency of C_i differs in the non-loss and soil-loss tests. In the non-loss test, the C_i value is small and increases and then decreases with ΔH due to the accumulated fine sand from the storerooms before and migrated particles to the storerooms behind. However, due to the data lack of C_5

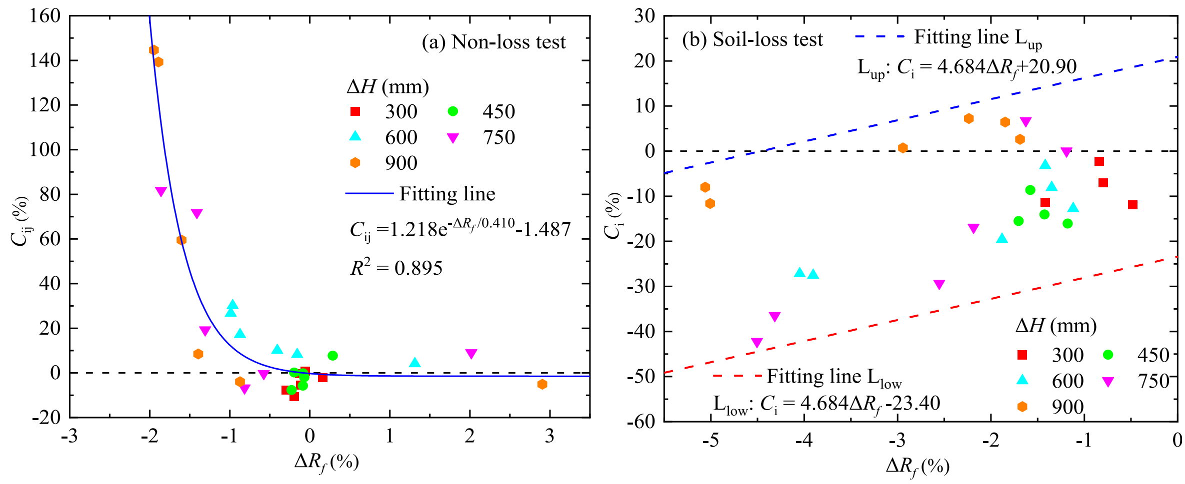

Fig. 19. Relationship between ΔR_f and C_i: (a) Non-loss test, and (b) Soil-loss test.

and C_6 when ΔH is 300 mm and 450 mm, only a part of the variation tendency of C_i in the soil-loss test is presented. The value of C_i in the soil-loss test decreases first and then increases when ΔH increases from 600 mm to 900 mm. Since the clogging phenomenon around the horizontal seam of storeroom S_7 is more severe than in other cases, the decrease in Q results in a smaller absolute value of C_i when ΔH is 900 mm. Due to the data lack, C_7 in the soil-loss test cannot be present, indicating the same tendency as C_6 in the soil-loss test because of the local clogging phenomenon around the horizontal seam. Deng et al. (2020) studied the variation in k_i along seepage path in horizontal seepage under soil-loss test, where the result accord with the tendency that the minimum value of C_i occurs at middle position along seepage path and maximum value of C_i occurs at position closed to soil-loss boundary.

5.3. Relationship between ΔR_f and C_i

Fig. 19 shows the relationship between ΔR_f and C_i in the non-loss and soil-loss tests. Due to the boundary effect in the non-loss boundary test, ΔR_f in storeroom S_7 and data of C_7 in the non-loss test are eliminated. The value of C_i can be fitted using the exponential function (Fig. 19a), where C_i decreases with the increasing ΔR_f. When ΔH is relatively low (300 mm or 450 mm), the C_i values concentrate on the area around the origin, indicating that the suffusion process and the permeability variation are small. Other values are distributed on both sides of the fitting line, and the permeability variation increases with the increasing ΔH. By this equation, the value of ΔR_f can predict C_i.

In the soil-loss boundary test, the variation tendency of C_i differs from that in the non-loss boundary test, indicating that the boundary condition significantly affects the soil permeability. Fig. 19b shows that the value of C_i increases with the increase in ΔR_f, and the scatters of C_i distribute concentratedly in an area limited by two parallel lines. The parallel lines' slopes are obtained using the least squares method, obtaining the area with a 95% prediction band, of which the upper and lower bound lines can be obtained. The equation of the upper and lower bound lines can predict the upper and lower values of C_i using the value of ΔR_f.

6. Conclusions

This study conducted a horizontal experiment with non-loss and soil-loss boundaries to analyze the permeability variation of gap-graded soil after suffusion. The change content of fine sand (ΔR_f) and change rate of hydraulic conductivity of soils in each storeroom (C_i) are analyzed after soil-loss and non-loss tests, respectively. The following conclusions are obtained:

(1) The experiment apparatus includes a water tank, a horizontal cylinder, water-level monitoring tubes, and a water-collect box. Soil samples are filled into seven soil storerooms (labeled from S_1 to S_7 from upstream to downstream). A round plate with a filter screen or horizontal seam controls the non-loss or soil-loss boundaries. The hydraulic head difference (ΔH) varies during suffusion.
(2) In the non-loss test, the soil sample filling areas along the seepage path are divided into the runoff area (storerooms S_1 to S_4), the transited area (storeroom S_5), and the accumulated area (storerooms S_6 to S_7) according to the negative or positive values of ΔR_f. C_i decreases from the runoff area to the transited area and rebounds in the accumulated area.
(3) In the soil-loss test, all soil sample filling areas are in the runoff area, where the gentle-loss part (storerooms S_1 to S_4), the strengthened-loss part (storerooms S_5 to S_6), and the alleviated-loss part (storeroom S_7) are further divided according to the loss degree of fine sand. C_i increases and then decreases along the seepage path.
(4) Comparing the results of ΔR_f and C_i in the non-loss and soil-loss tests, similar-effect and reverse-effect areas due to the boundary condition can be divided. The ΔR_f and C_i present similar variation tendencies in the corresponding similar-effect area and transfer to the opposite tendency in the reverse-effect area.
(5) The relationship between C_i and ΔR_f differs with the boundary condition. C_i exponentially decreases with the increasing ΔR_f in the non-loss test, whereas C_i distributes in a bond zone limited by two parallel lines in the soil-loss test.

Declaration of competing interest

The authors declare that they have no known competing financial interests or personal relationships that could have appeared to influence the work reported in this paper.

Acknowledgments

The research work described herein was funded by the National Nature Science Foundation of China (Grant No. 41877213). This financial support is gratefully acknowledged.

References

ASTM D2487, 2011. Standard Practice for Classification of Soils for Engineering Purposes (Unified Classification System). ASTM International, West Conshohocken, PA, USA.
Benamar, A., Correia-dos-Santos, R.N., Bennabi, A., Karoui, T., 2019. Suffusion evaluation of coarse-graded soils from Rhine dikes. Acta Geotech 14, 815–823.
Caldeira, L., 2019. Internal erosion in dams: studies and rehabilitation. Int. J. Civ. Eng. 17, 457–471.
Chen, C., Zhang, L.M., Chang, D.S., 2016. Stress–strain behaviour of granular soils subjected to internal erosion. J. Geotech. Geoenviron. Eng. 142 (12), 6016014.
Chen, L., Wan, Y., He, J.J., Luo, C.M., Yan, S.F., He, X.F., 2021. Experimental study on the suffusion mechanism of gap-graded soils under an exceedance hydraulic gradient. Nat. Hazards 109, 405–439.
Cheng, W.C., Ni, J.C., Shen, S.L., 2017. Experimental and analytical modeling of shield segment under cyclic loading. Int. J. GeoMech. 17 (6), 04016146.
Cheng, W.C., Ni, J.C., Shen, S.L., Wang, Z.F., 2018. Modeling of permeation and fracturing grouting in sand: laboratory investigations. J. Test. Eval. 46 (5), 2067–2082.
Deng, G., Zhang, L.L., Chen, R., Liu, L., Shu, K.X., Zhou, Z.L., 2020. Experimental investigation on suffusion characteristics of cohesionless soils along horizontal seepage flow under controlled vertical stress. Front. Earth Sci. 8, 195.
Dong, Y., Fatahi, B., Khabbaz, H., Zhang, H., 2018. Influence of particle contact models on soil response of poorly graded sand during cavity expansion in discrete element simulation. J. Rock Mech. Geotech. Eng. 10 (6), 1154–1170.
Fetrati, M., Pak, A., 2020. Numerical simulation of sanding using a coupled hydro-mechanical sand erosion model. J. Rock Mech. Geotech. Eng. 12 (4), 811–820.
Foster, M., Fell, R., Spannagle, M., 2000. The statistics of embankment dam failures and accidents. Can. Geotech. J. 37, 1000–1024.
Hosn, R.A., 2017. Suffusion and its Effects on the Mechanical Behavior of Granular Soils: Numerical and Experimental Investigations. Universite Grenoble Alpes, UGA, France.
Ke, L., Takahashi, A., 2014a. Experimental investigations on suffusion characteristics and its mechanical consequences on saturated cohesionless soil. Soils Found. 54 (4), 713–730.
Ke, L., Takahashi, A., 2014b. Triaxial erosion test for evaluation of mechanical consequences of internal erosion. Geotech. Test J. 37 (2), 347–364.
Kim, I., Lee, H.J., Chung, C.K., 2022. Assessing the internal erosion sensitivity of earth fill dam soils based on the phenomena of suffusion and suffusion. Nat. Hazards 113, 1471–1493.
Li, P.N., Xu, Y.S., Wang, X.W., 2023. Estimation of hydraulic conductivity by the modified Kozeny–Carman equation considering the derivation principle of the original equation. J. Hydrol. (Wellingt. North) 621, 129658.
Liang, Y., Yeh, T.C.J., Wang, J.J., Liu, M.W., Zha, Y.Y., Hao, Y.H., 2019. Onset of suffusion in upward seepage under isotropic and anisotropic stress conditions. Eur. J. Environ. Civ. Eng. 23 (12), 1520–1534.
Liang, Y., Yeh, T.C.J., Ma, C., Zhang, Q., Yang, D.H., Hao, Y.H., 2020. Experimental investigation of internal erosion behaviours in inclined seepage flow. Hydrol. Process. 34 (26), 5315–5326.
Liang, Y., Sun, Z.W., Zhang, Q., 2022. Experimental study of the internal erosion behaviors of granular soils in horizontal seepage. Mater. Tehnol. 56 (1), 59–64.
Luo, Y., Luo, B., Xiao, M., 2019. Effect of deviator stress on the initiation of suffusion. Acta Geotech 15 (6), 1607–1617.
Luo, Y.L., Zhang, X.J., Xiao, M., 2020. Influence of constriction-based retention ratio on suffusion in double-layered alluvial foundation with a cutoff wall. Soils Found. 60 (6), 1489–1506.
Lyu, H.M., Shen, S.L., Wu, Y.X., Zhou, A.N., 2021. Calculation of groundwater head distribution with a close barrier during excavation dewatering in confined aquifer. Geosci. Front. 12 (2), 791–803.
Lyu, H.M., Shen, S.L., Zhou, A.N., Yin, Z.Y., 2022. Assessment of safety status of shield tunnelling using operational parameters with enhanced SPA. Tunn. Undergr. Space Technol. 123, 104428.
Ma, D., Duan, H.Y., Li, X.B., Li, Z.H., Zhou, Z.L., Li, T.B., 2019. Effects of seepage-induced erosion on nonlinear hydraulic properties of broken red sandstones. Tunn. Undergr. Space Technol. 91, 102993.
Moffat, R.A., Fannin, R.J., 2006. A large permeameter for study of internal stability in cohesionless soils. Geotech. Test J. 29 (4), 273–279.
Pachideh, V., Hosseini, S.M.M.M., 2018. A new physical model for studying flow direction and other influencing parameters on the internal erosion of soils. Geotech. Test J. 42 (6), 20170301.
Peng, S.G., Rice, J.D., 2020. Inverse analysis of laboratory data and observations for evaluation of backward erosion piping process. J. Rock Mech. Geotech. Eng. 12 (5), 1080–1092.
Planes, T., Mooney, M.A., Rittgers, J.B.R., Parekh, M.L., Behm, M., Snieder, R., 2016. Time-lapse monitoring of internal erosion in earthen dams and levees using ambient seismic noise. Geotechnique 66 (4), 301–312.
Rochim, A., Marot, D., Sibille, L., Le, V.T., 2017. Effects of hydraulic loading history on suffusion susceptibility of cohesionless soils. J. Geotech. Geoenviron. Eng. 143 (7), 04017025.
Sail, Y., Marot, D., Sibille, L., Alexis, A., 2011. Suffusion tests on cohesionless granular matter. Eur. J. Environ. Civ. Eng. 15 (5), 799–817.
Selvadurai, A.P.S., Głowacki, A., 2018. Estimates for the local permeability of the Cobourg limestone. J. Rock Mech. Geotech. Eng. 10 (6), 1009–1019.
Shire, T., O'Sullivan, C., Hanley, K., Fannin, R., 2014. Fabric and effective stress distribution in internally unstable soils. J. Geotech. Geoenviron. Eng. 140 (12), 04014072.
Sibille, L., Marot, D., Sail, Y., 2015. A description of internal erosion by suffusion and induced settlements on cohesionless granular matter. Acta Geotech 10 (6), 735–748.
Tan, Y., Lu, Y., 2017. Forensic diagnosis of a leaking accident during excavation. J. Perform. Constr. Facil. 31 (5), 04017061.
Tan, Y., Long, Y.Y., 2021. Review of cave-in failures of urban roadways in China: a database. J. Perform. Constr. Facil. 35 (6), 04021080.
Tang, G.H., Wang, N.D., Liu, S.T., Jie, Y.X., 2023. Experimental study on the influence of filter mesh size on radial permeability of sand. J. Beijing Univ. Aeronaut. Astronaut. 49 (6), 1516–1522 (in Chinese).
Wang, T., Zhang, F.S., Furtney, J., Damjanac, B., 2022. A review of methods, applications and limitations for incorporating fluid flow in the discrete element method. J. Rock Mech. Geotech. Eng. 14 (3), 1005–1024.
Wang, X.W., Yang, T.L., Xu, Y.S., Shen, S.L., 2019. Evaluation of optimized depth of waterproof curtain to mitigate negative impacts during dewatering. J. Hydrol. 577, 123969.
Wang, X.W., Xu, Y.S., 2021. Impact of the depth of diaphragm wall on the groundwater drawdown during foundation dewatering considering anisotropic permeability of aquifer. Water 13 (4), 418.
Wang, X.W., Xu, Y.S., 2022. Investigation on the phenomena and influence factors of urban ground collapse in China. Nat. Hazards 113, 1–33.
Wang, X.W., Xu, Y.S., 2023. Permeability property variation in sandy soil induced by suffusion via a horizontal seepage laboratory test. Acta Geotech 18 (10), 5285–5298.
Wu, H.N., Shen, S.L., Liao, S.M., Yin, Z.Y., 2015. Longitudinal structural modelling of shield tunnels considering shearing dislocation between segmental rings. Tunn. Undergr. Space Technol. 50, 317–323.
Wu, H.N., Shen, S.L., Yang, J., 2017. Identification of tunnel settlement caused by land subsidence in soft deposit of Shanghai. J. Perform. Constr. Facil. 31 (6), 04017092.
Wu, H.N., Shen, S.L., Chen, R.P., Zhou, A.N., 2020a. Three-dimensional numerical modelling on localised leakage in segmental lining of shield tunnels. Comput. Geotech. 122, 103549.
Wu, Y.X., Lyu, H.M., Shen, S.L., Zhou, A.N., 2020b. A three–dimensional fluid–solid coupled numerical modeling of the barrier leakage below the excavation surface due to dewatering. Hydrogeol. J. 28 (3), 1449–1463.
Wu, Y.X., Shen, S.L., Lyu, H.M., Zhou, A.N., 2020c. Analysis of leakage effect of waterproof curtain during excavation dewatering. J. Hydrol. 583, 124582.
Xiao, M., Shwiyhat, N., 2012. Experimental investigation of the effects of suffusion on physical and geomechanic characteristics of sandy soils. Geotech. Test J. 35 (6), 890–900.
Xu, Y.S., Ma, L., Shen, S.L., Sun, W.J., 2012. Evaluation of land subsidence by considering underground structures that penetrate the aquifers of Shanghai, China. Hydrogeol. J. 20, 1623–1634.
Xu, Y.S., Shen, S.L., Du, Y.J., Chai, J.C., Horpibulsuk, S., 2013. Modelling the cutoff behavior of underground structure in multi-aquifer-aquitard groundwater system. Nat. Hazards 66 (2), 731–748.
Xu, Y.S., Shen, S.L., Ma, L., Sun, W.J., Yin, Z.Y., 2014. Evaluation of the blocking effect of retaining walls on groundwater seepage in aquifers with different insertion depths. Eng. Geol. 183, 254–264.
Xu, Y.S., Yan, X.X., Shen, S.L., Zhou, A.N., 2019. Experimental investigation on the blocking of groundwater seepage from a waterproof curtain during pumped dewatering in an excavation. Hydrogeol. J. 27 (7), 2659–2672.
Yang, J., Yin, Z.Y., Laouafa, F., Hicher, P.Y., 2019a. Analysis of suffusion in cohesionless soils with randomly distributed porosity and fines content. Comput. Geotech. 111, 157–171.
Yang, J., Yin, Z.Y., Laouafa, F., Hicher, P.Y., 2019b. Modeling coupled erosion and filtration of fine particles in granular media. Acta Geotech 14, 1615–1627.
Yang, J., Yin, Z.Y., Laouafa, F., Hicher, P.Y., 2022. Numerical analysis of internal erosion impact on underground structures: application to tunnel leakage. Geomech. Energy Environ. 31, 100378.
Yin, Z.Y., Yang, J., Laouafa, F., Hicher, P.Y., 2020. A framework for coupled hydro-mechanical continuous modelling of gap-graded granular soils subjected to suffusion. Eur. J. Environ. Civ. Eng. 1, 1–22.
Yin, Z.Y., Wang, P., 2021. Micro-mechanical analysis of caisson foundation in sand using DEM: particle shape effect. Appl. Ocean Res. 111, 102630.
Zeng, C.F., Liao, H., Xue, X.L., et al., 2022. Responses of groundwater and soil to dewatering considering the barrier effect of adjacent metro station on multi-aquifers. J. Hydrol. 612, 128117.

Zeng, C.F., Powrie, W., Xue, X.L., Li, M.K., Mei, G.X., 2021a. Effectiveness of a buttress wall in reducing retaining wall movement during dewatering before bulk excavation. Acta Geotech 16, 3253–3267.
Zeng, C.F., Xue, X.L., Li, M.K., 2021b. Use of cross wall to restrict enclosure movement during dewatering inside a metro pit before soil excavation. Tunn. Undergr. Space Technol. 112, 103909.
Zhang, D.M., Gao, C.P., Yin, Z.Y., 2019. CFD-DEM modeling of seepage erosion around shield tunnels. Tunn. Undergr. Space Technol. 83, 60–72.
Zhong, C.H., Le, V.T., Bendahmane, F., Marot, D., Yin, Z.Y., 2018. Investigation of spatial scale effects on suffusion susceptibility. J. Geotech. Geoenviron. Eng. 144 (9), 04018067.

Yeshuang Xu obtained her BSc degree in Civil Engineering from Suzhou University of Science and Technology, China, in 1999, and her MSc degree and PhD in Civil Engineering from Shanghai Jiao Tong University in 2006 and 2010, respectively. She was affiliated as assistant professor from 2010 to 2013 and associate professor since 2014 with Shanghai Jiao Tong University, China. Her research interests include (1) Mechanism and simulation study on land subsidence; and (2) Research on engineering, geological and environmental problems related to groundwater seepage. She has been participated in some projects funded by National Nature Science Foundation of China.